buildings

MDPI

Article

Machine Learning and Regression Models for Evaluating Ultimate Performance of Cotton Rope-Confined Recycled Aggregate Concrete

Kittipoom Rodsin [1], Ali Ejaz [2], Huaping Wang [3], Panumas Saingam [4], Panuwat Joyklad [5], Wasim Khaliq [2], Qudeer Hussain [1] and Chichaya Boonmee [6,*]

[1] Center of Excellence in Structural Dynamics and Urban Management, Department of Civil and Environmental Engineering Technology, College of Industrial Technology, King Mongkut's University of Technology North Bangkok, Bangkok 10800, Thailand; kittipoom.r@cit.kmutnb.ac.th (K.R.); ebbadat@hotmail.com (Q.H.)
[2] National Institute of Transportation, National University of Sciences and Technology (NUST), Islamabad 44000, Pakistan; enggaliejax@gmail.com (A.E.); wasimkhaliq@nice.nust.edu.pk (W.K.)
[3] School of Civil Engineering and Mechanics, Lanzhou University, Lanzhou 730000, China; wanghuaping1128@sina.cn
[4] Department of Civil Engineering, School of Engineering, King Mongkut's Institute of Technology Ladkrabang, Bangkok 10520, Thailand; panumas.sa@kmitl.ac.th
[5] Department of Civil and Environmental Engineering, Srinakharinwirot University, Nakhonnayok 26120, Thailand; panuwatj@g.swu.ac.th
[6] Department of Teacher Training in Civil Engineering, Faculty of Technical Education, King Mongkut's University of Technology North Bangkok, Bangkok 10800, Thailand
* Correspondence: chichaya.b@fte.kmutnb.ac.th

Abstract: This study investigates the use of cotton ropes (CRs) as a sustainable and cost-effective substitute for synthetic fiber-reinforced polymers for concrete confinement, offering significant environmental benefits such as lower CO_2 emissions and reduced energy consumption. The work evaluates the effectiveness of CR strips for confining concrete, including scenarios with recycled concrete aggregates (ReCA). Compressive strength improvements varied among specimens, with Specimen I-3F showing a 140.52% increase and Specimen II-3F achieving a 46.67% improvement. Strip configurations for Type I recycled aggregate concrete (RAC) outperformed full wraps on Type II RAC, exemplified by Specimen I-3S's 84.51% improvement. Ultimate strain enhancements ranged from 915% to 4490.91%, driven by the significant rupture strain of cotton rope confinement. For Type I RAC, complete wrapping significantly outperformed strip configurations by 56%, 50%, and 32% in ultimate strength improvement for 1, 2, and 3 layers, respectively. The confinement ratio, varying from 0.10 to 0.70, greatly influenced the compressive behavior, with compressive strength normalized by unconfined strength increasing consistently with the confinement ratio. A minimum confinement ratio of roughly 0.40 is required to achieve an increasing second part in the compressive behavior. The initial parabolic branch was modeled using Popovics' formulation, revealing an elastic modulus approximately 20% lower than ACI 318-19 predictions. The second branch was described using a linear approximation, and nonlinear regression analysis produced expressions for key points on the idealized compressive curve, enhancing model accuracy for CR-confined RAC. The R^2 values for the nonlinear regression analysis performed on experimental results were greater than 0.90. This study highlights the effectiveness of neural network expressions to predict the compressive strength of CR-confined concrete. A strength reduction (ratio of full wrap and strip wrap height CRs) factor of 0.67 was proposed and used for strip-wrapped specimens. It was seen that the neural network models also predicted the compressive strength of partially wrapped specimens with reasonable accuracy using the strength reduction factor.

check for updates

Academic Editor: Grzegorz Ludwik Golewski

Received: 19 November 2024
Revised: 23 December 2024
Accepted: 25 December 2024
Published: 28 December 2024

Citation: Rodsin, K.; Ejaz, A.; Wang, H.; Saingam, P.; Joyklad, P.; Khaliq, W.; Hussain, Q.; Boonmee, C. Machine Learning and Regression Models for Evaluating Ultimate Performance of Cotton Rope-Confined Recycled Aggregate Concrete. *Buildings* **2025**, *15*, 64. https://doi.org/10.3390/buildings15010064

Copyright: © 2024 by the authors. Licensee MDPI, Basel, Switzerland. This article is an open access article distributed under the terms and conditions of the Creative Commons Attribution (CC BY) license (https://creativecommons.org/licenses/by/4.0/).

Keywords: cotton; compressive behavior; recycled aggregates; neural networks; regression

1. Introduction

Recently, rapid urbanization has significantly enhanced demolition and construction activities, leading to the creation of vast magnitudes of construction and demolition (C&D) waste, particularly concrete waste. This surge in C&D waste poses a profound effect on both the environment and society. Massive-scale reuse of C&D waste has been recognized as the most efficient answer to mitigating the escalating issue of waste dumping by landfilling [1,2]. Utilizing recycled aggregates presents a sustainable alternative to decrease the construction industry's reliance on natural aggregates (NatA), which are becoming increasingly scarce, especially with the expansion of major urban areas [3,4].

With rapid global urbanization, concrete has become a key material in the construction of buildings, roads, and various civil engineering infrastructures [5,6]. However, when the service life ends, concrete typically turns into C&D, which is often transported for piling and landfilling [7,8]. C&D is composed of a mix of heavy substances like concrete, wood, metal, gypsum, and plastic, with concrete being the predominant debris [9]. NaTA, which constitutes about 60% of the mass in concrete blends [10], is embedded within recycled concrete aggregates (ReCA) when dismantled concrete is prepared for reuse. However, ReCA differs from NaTA, which is ascribed to the occurrence of cement mortar adhering to its surface, which leads to higher water absorption, increased crushing susceptibility, and variations in the interfacial zones [11]. Consequently, ReCA tends to have inferior properties compared to NaTA, which can negatively impact the engineering performance of materials like asphalt concrete that incorporate ReCA [12,13].

Over the past 40 years, extensive research has focused on incorporating RA into recycled aggregate concrete (RAC) [14]. While RAC offers both benefits and challenges, it has been shown to significantly improve the sustainability of concrete manufacturing [15,16]. However, the poor properties of ReCA, such as low density, high water absorption, and elevated crushing value [17–19], lead to several shortcomings in RAC, including lower mechanical strength, greater shrinkage, and reduced durability [20,21]. The primary issue with ReCA is the old mortar that remains attached to the original aggregate, which creates a weak interfacial transition zone (ITZ) [22–24]. Several methods have been explored to address this issue, such as removing the adhered mortar. For example, Li et al. [25] used a calcination-ball milling technique to decrease water absorption, while Wang et al. [26] applied mechanical rubbing to ReCA soaked in acetic acid to decrease the mortar adhesion and water absorption. Other techniques, such as heating [18], ultrasonic treatment [24], and microwaving [22], have also been effective in mortar removal. Despite their success, these methods require complex processes, costly equipment, and high energy utilization, which contradict the goal of sustainability. Additionally, the peeling method can often induce internal damage to the ReCA [27].

In current years, fiber-reinforced polymer (FRP) has attained widespread acceptance in structural strengthening applications ascribed to their high strength-to-weight ratio, corrosion endurance, and installation easiness [28]. The strength-to-weight ratio of FRPs is significantly higher in comparison to traditional reinforcement methods that use steel or reinforced concrete (RC) jackets, making FRPs a more efficient option for enhancing structural performance without adding excessive weight [29]. Moreover, FRPs provide outstanding endurance against corrosion, which renders them particularly appropriate for utilization in harsh conditions where conventional materials like steel are prone to deterioration over time [30]. Subsequently, various strengthening uses of FRPs have been investigated in

recent years, including flexural reinforcement [31–35], shear enhancement [36–39], substandard lap splice strengthening [40–44], and enhancement of the compressive behavior of concrete [45–48]. Works comprising experimental or analytical domains have shown that FRP strengthening greatly enhances the strength and ultimate strain of the compressive response of concrete. Various stress vs. strain expressions are accessible for predicting the behavior of FRP-confined concrete, valid for both circular and non-circular cross-sectional shapes, further validating its effectiveness in structural strengthening [49,50]. These expressions have contributed to a thorough sense of the compressive response of FRP-confined concrete.

The price of synthetic FRPs may be reasonably expensive, with prices approaching approximately 150 USD per square meter of single-layer [51]. Additionally, the making of synthetic fibers needs large magnitudes of fossil gases and includes high energy utilization [52]. For example, creating one ton of carbon fiber consumes around 300 gigajoules of energy, whereas manufacturing the same level of natural hemp fiber needs only approximately 5 gigajoules [53]. This significant energy demand converts into a large carbon footprint, with the manufacturing of one ton of Carbon Fiber Reinforced Polymer (CFRP) emitting about 29,000 kg of CO_2. In comparison, one ton of glass fiber results in releases ranging from 1700 to 2500 kg of CO_2. Natural fibers, like jute, hemp, and kenaf, offer a more sustainable alternative, with emissions of about 550, 400, and 410 kg of CO_2-equivalent per ton of fiber, respectively [54]. Moreover, the making of synthetic FRPs produces hazardous derivatives that can induce health hazards due to exposure to specific chemicals [55–57]. The disposal of synthetic FRPs also exhibits environmental issues, as they cannot be recycled [58]. Despite these drawbacks, the demand for FRPs has steadily increased since their introduction, with the construction industry accounting for roughly 10% of the worldwide demand [59].

In current times, large rupture strain confinement has represented a notable advancement in structural reinforcement. Conventional FRP-strengthened RC columns frequently fail owing to FRP failure. Nevertheless, RC columns strengthened by using large rupture strain FRPs, which demonstrate rupture strains surpassing 5%, show improved endurance against failure and enhanced seismic response [60,61]. Similarly, cotton ropes (CRs), like synthetic FRPs, provide passive confinement but become active during substantial lateral deformations of the concrete core. The high rupture strain of CRs is crucial because it allows the concrete core to undergo substantial lateral deformation, thereby significantly improving the compressive ductility of the concrete. Large rupture strain FRPs demonstrate enhanced deformation capacity and energy dissipation compared to conventional FRPs when applied as lateral confinement of concrete columns under similar confinement conditions [60,62–64]. Previous research on natural FRP confinement has predominantly focused on full confinement, with partial confinement approaches, such as using strips, still largely unexplored. Partial confinement offers several advantages, including reduced material requirements and simpler, faster application compared to full confinement [65]. This approach can be particularly beneficial for current concrete columns with steel ties at large spacing, as it enhances the columns' response by providing additional support among the sparse ties, effectively mitigating local buckling of longitudinal steel rebars [66]. Furthermore, exerting partial strengthening to weakened sections of concrete columns may substantially boost their ultimate capacities without the necessity of confining the entire column [67].

Exploring cotton ropes (CRs) as a replacement for synthetic FRPs is critical for advancing sustainable construction practices. CRs offer a cost-effective and eco-friendly solution, generating substantially lower CO_2 releases and requiring less energy during manufacturing. Their widespread availability and high rupture strain further enhance their

suitability for structural applications. However, the potential of partial confinement using CR strips remains underexplored. This work addresses this research gap by evaluating the effectiveness of CR strips in confining concrete, including cases with partial or full substitution of natural coarse aggregates by using ReCA. By comparing CR strip behavior with full wrapping systems and forming analytical expressions, this study aims to deepen understanding and provide predictive tools for optimizing CR usage in increasing concrete structural performance.

2. Experimental Details

2.1. Details of Specimens

The effectiveness of CR confinement was assessed by performing a comprehensive experimental program on circular concrete samples. All samples measured 300 mm in height and 150 mm in diameter. Table 1 shows the information on all samples employed in this work. It is noteworthy that 50 NA in concrete was substituted with RecA. A total of two groups were tested. Specimens in both groups were fabricated by a 50% replacement of NatA with RecA. Moreover, samples in Group 1 and Group 2 were confined with fully wrapped CRs, i.e., without any discontinuity and strip configuration of CR, respectively. Figure 1 shows the strengthening configurations adopted in this work. Both groups comprised eight specimens each. Out of those eight specimens, four specimens each were fabricated with a target compressive strength of either 15 MPa or 25 MPa. A two-part nomenclature was used to recognize samples, with the first and second representing the target compressive strength (I for 15 MPa and II for 25 MPa) and number of strengthening layers (F for full and S for strips), respectively. Thus, for instance, the name I-1S represented a specimen fabricated with a target compressive strength of 15 MPa and strengthened in a strip configuration with one CR layer.

Table 1. Details of cylinders used in this work.

Group	Name	Strengthening Configuration	Layer	Target Concrete Strength (MPa)
1	I-C	None	None	15
	I-1F	Full	1	15
	I-2F	Full	2	15
	I-3F	Full	3	15
	II-C	None	None	25
	II-1F	Full	1	25
	II-2F	Full	2	25
	II-3F	Full	3	25
2	I-C	None	None	15
	I-1S	Strip	1	15
	I-2S	Strip	2	15
	I-3S	Strip	3	15
	II-C	None	None	25
	II-1S	Strip	1	25
	II-2S	Strip	2	25
	II-3S	Strip	3	25

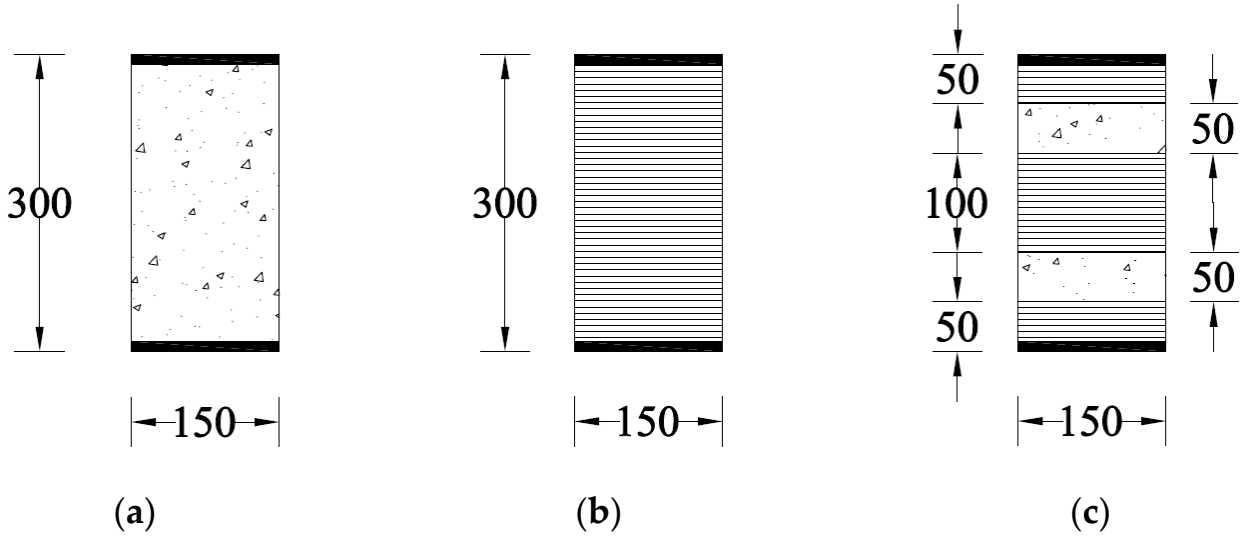

Figure 1. Sample information and strengthening patterns: (**a**) control, (**b**) full strengthening, and (**c**) strip strengthening.

2.2. Material Properties

Cotton ropes, readily available locally, were used in this work. The cotton rope was acquired from Nanacenter Supply, Bangkok, Thailand. Each rope had a diameter of 2.4 mm and a tensile capacity of 129.3 MPa, with an ultimate fracture strain of 13.3%. The standard tensile strengths were carried out to find the tensile capacity and strain of cotton rope. The cotton ropes were impregnated with epoxy and tested in a Testometeric (The Testometric Co., Ltd., Rochdale, UK) universal testing machine following ASTM standards [68]. Polyester resin was applied, offering tensile and flexural strengths of 55 MPa and 80 MPa, respectively. The resin's ultimate elongation was 2.5%, and its curing time varied between 6 and 10 min. The coarse aggregates utilized had an upper size limit of 19.5 mm. Figure 2 illustrates the typical cotton ropes employed in the study. Material properties are given in Table 2.



Figure 2. Typical cotton ropes utilized for strengthening.

Table 2. Characteristics of strengthening materials.

Material	Diameter (mm)	Tensile Capacity (MPa)	Fracture Strain (%)	Flexural Capacity (MPa)	Curing Duration (min)
Cotton	2.4	129.3	13.3	-	-
Resin	-	55.0	2.5	80.0	5–15

2.3. Strengthening Process

A 28-day curing period was practiced before the onset of strengthening. It is noteworthy that the wet layup process, as suggested by ACI SPEC-440 [69], was adopted for the strengthening application. To attach the cotton ropes, a wet layup process was utilized. Initially, polyester resin was used on the concrete surface utilizing a hand brush. The cotton ropes were then manually placed onto the resin-coated surface, as depicted in Figure 3. For specimens requiring multiple layers of reinforcement, each wrap was allowed to dry for 24 h before applying the next. The dried layer was coated with polyester resin, following the addition of another layer of cotton ropes. The method was iterated until the required quantity of confinement was acquired.



Figure 3. Process of constructing samples: (**a**) wrapping cotton rope, (**b**) application of polyester resin on cotton ropes for wrapping next wraps, and (**c**) confined full wrap samples.

2.4. Experimental Setup

The compressive setup was carried out by adopting ASTM C39 [53], with all samples undergoing a monotonic application of loads. A 500 kN capacity Universal Testing Machine (UTM) was employed in this work. Two LVDTs were positioned on each side of the samples, with the tip of each LVDT touching the top surface of the UTM. To prevent premature failure, a steel clamp was applied at each end of the cylinders. The displacement transducer readings were employed to calculate compressive strain, while the applied load was used to find the resulting compressive stress. The axial deformation measured at each step was divided by the initial height of the cylinders to determine the compressive strain. The typical test configuration is shown in Figure 4.

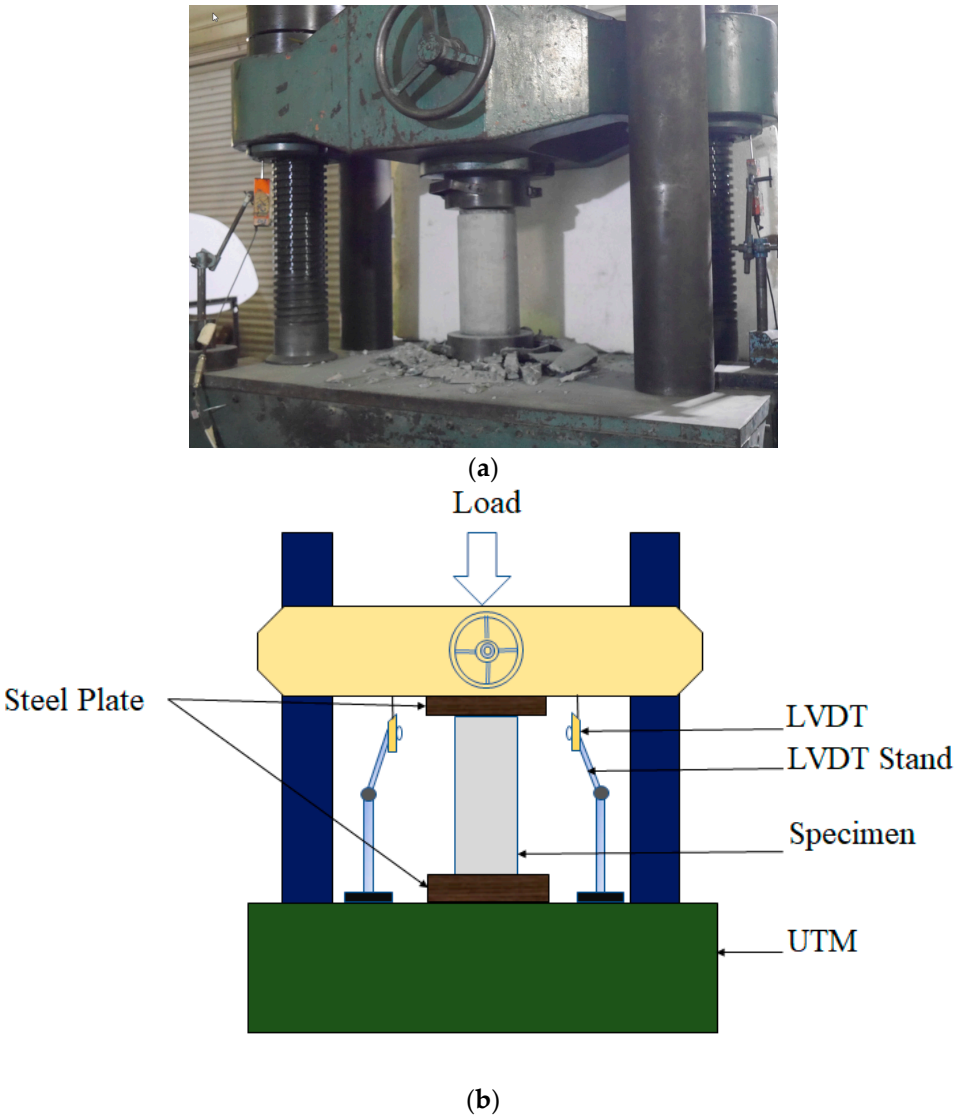

Figure 4. Adopted test configuration: (**a**) actual and (**b**) diagram.

3. Experimental Findings

3.1. Observed Failure Patterns

The failure patterns of the typical samples are shown in Figures 5 and 6, corresponding to samples with 50% and 100% replacement of natural aggregates (NA), respectively. In all cases, the specimens failed due to the fracture of the cotton rope strips near the mid-height of the samples. During testing, preliminary cracking appeared in the visible concrete sections among the cotton rope reinforcements as the exerted load neared the strength

level of unstrengthened concrete. With a further increase in load, these cracks spread, resulting in substantial spalling of the concrete surface. A sudden rupture of the cotton rope strips followed, supplemented by a discrete explosive noise, signifying an instant emission of energy. This abrupt fracture marked the critical failure of the samples. After the failure of the cotton strips, the concrete core experienced acute crushing, with some fragments remaining affixed to the failed strips, representing a durable bonding between the cotton ropes and concrete. This progression of failure progressed from original cracking to ultimate fracture and crushing, consistent with failure patterns observed in previous studies on FRP strip strengthening [70,71]. The most extensive concrete crushing occurred in specimens with three wraps of cotton strips. As Zeng et al. [71] noted, enhancing the number of wraps enhances effective confinement, which in turn raises axial stress, creating a stronger potential for concrete crushing between the strips. For fully wrapped specimens, failure was started by the fracture of cotton ropes near the middle of the height. In samples with multiple layers, the rupture followed a progressive pattern, as evidenced by snapping sounds, indicating the sequential failure of the underlying layers. Typical cracks are shown in Figure 7.



Figure 5. Observed failure modes in Group 1 and Group 2.



Figure 6. Observed failure modes in Group 3 and Group 4.

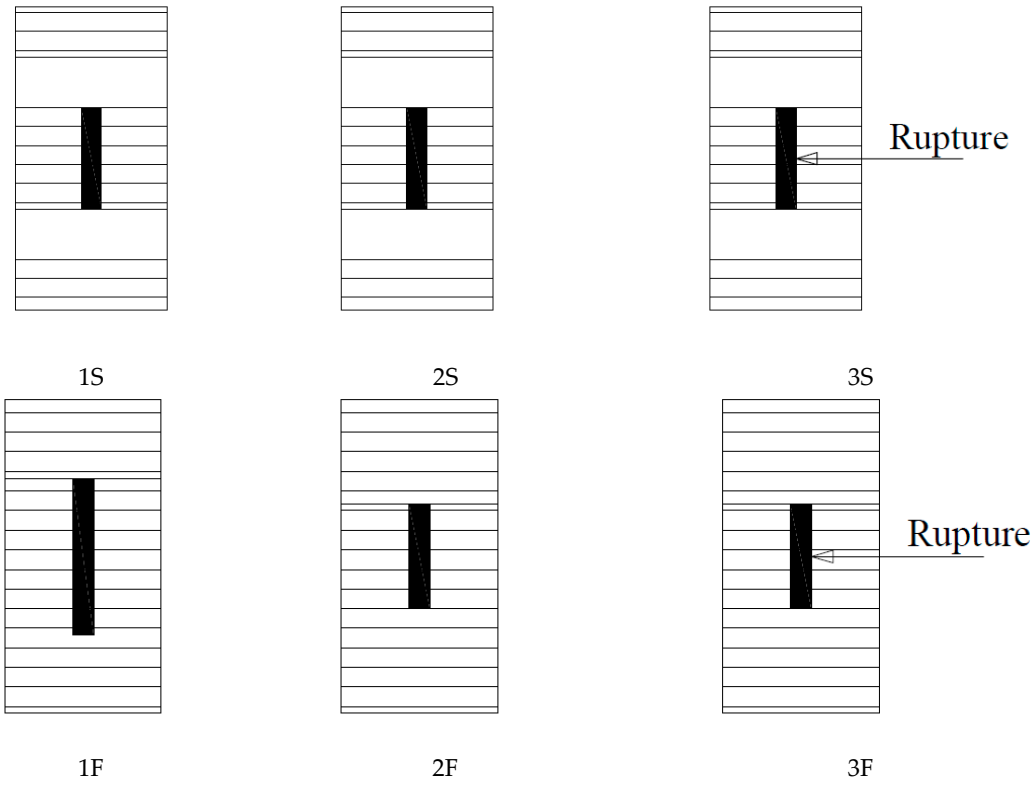

Figure 7. Typical failures of strip and full wraps.

3.2. Experimental Stress vs. Strain Relations

The compressive stress vs. strain responses of all samples are presented in Figure 8. To enhance clarity, the responses are separated for each group based on the strength of the unstrengthen concrete. Typically, the stress vs. strain curve comprises a stiff, elastic ascending branch that is characteristic of concrete behavior. This progression transitions into a parabolic curve, culminating in a secondary branch that can either ascend or descend depending on the confinement ratio. The confinement ratio is termed as the proportion of the confinement pressure employed by cotton FRPs to the compressive strength of unconfined concrete [72]. Consequently, the compressive stress vs. strain response of CR-confined concrete is idealized, as highlighted in Figure 8. It is noted that several key parameters are required to trace the response of CR-confined concrete, as highlighted in Figure 9. These parameters include the coordinates at the termination of the initial parabolic part, i.e., the stress f_{cc} (or f_{cu}) and strain ϵ_{cc}. The maximum compressive stress, hereby denoted as the compressive strength, in both failure modes is identified by the variable f_{cu}. Thus, the end of the initial parabolic branch of Type B failure becomes f_{cu}, whereas f_{cu} is identified at the end of the second ascending branch for Type A failure. Furthermore, the slope of the second branch Z is also a dominant factor in determining the nature of behavior. It is noteworthy that CR confinement imparted substantial ductility to RAC. The quantitative assessment of the improvement in ductility and compressive strength is presented in subsequent sections.

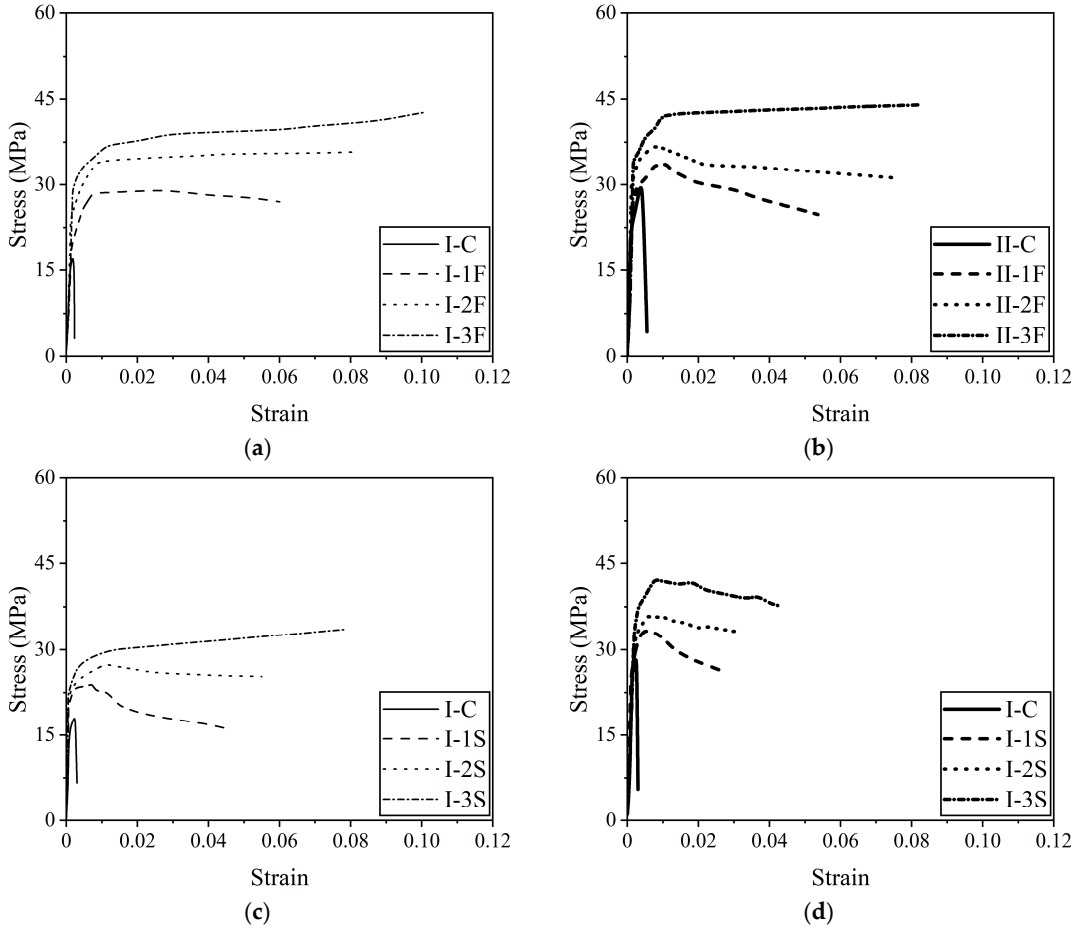

Figure 8. Experimental compressive stress vs. strain response: (**a**) concrete Type I with full configuration, (**b**) concrete Type II with full configuration, (**c**) concrete Type I with strip configuration, and (**d**) concrete Type II with strip configuration.

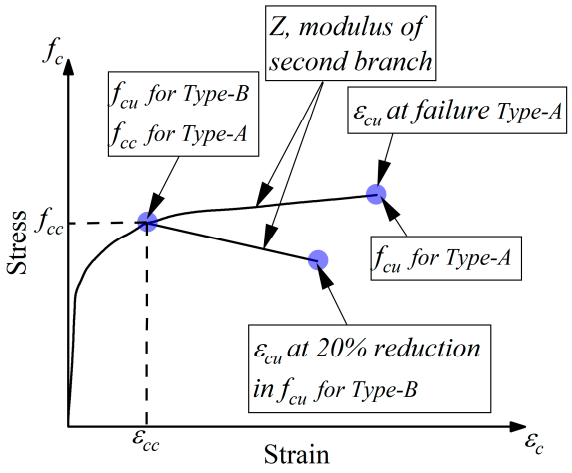

Figure 9. The idealized compressive behavior of CR-confined concrete.

3.3. Compressive Strength and Strain

It is noted that the ultimate strain in the case of Type B failure was identified, corresponding to a 20% reduction in compressive strength along the descending branch. The same parameter for Type A failure was noted at the termination of the second ascending branch. The percentage increase in the compressive strength and ultimate strain is presented in Table 3. It is observed that in terms of the percentage improvement in compressive strength, RAC Type I strengthened with complete CR wraps demonstrated the highest improvement. Specimen I-3F demonstrated up to 140.52% improvement in compressive strength. It is noted that the strip configuration applied on Type I RAC resulted in better improvement in the compressive strength than full configuration applied on Type II RAC. For example, Specimen I-3S showed an 84.51% improvement in compressive strength, whereas Specimen II-3F could only achieve a 46.67% improvement in compressive strength. This may be ascribed to the greater confinement ratio obtained in Specimen I-3S than in Specimen II-3F. The improvement in ultimate strain was phenomenal, ranging from 915% to 4490.91%, which can be related to the large fracture strain of CR confinement. Analogous to the compressive strength, the improvement in ultimate strain was significantly influenced by the confinement ratio. Clearly, specimens with Type I RAC in both groups demonstrated a greater improvement in general than that of Type II RAC. It is evident that the confinement effectiveness decreased in the strip pattern. Consequently, three of the four samples were designed with a full wrap configuration. Likewise, it is well established that higher unconfined compressive strength negatively impacts the effectiveness of the passive pressure applied. Therefore, three of the four samples were produced with lower unstrengthen strength. It shows that both the amount of confinement and the unstrengthened strength influenced the whole enhancements, which will be further examined in the following parts. It is further noted that the ultimate strain was substantially enhanced compared to the compressive strength. This can be attributed to the large rupture strain of cotton ropes that allowed the concrete to demonstrate large lateral deformations. Due to the Poisson's effect, the axial deformation capability of concrete was also enhanced significantly. Yuan et al. [73] utilized polyethylene terephthalate and polyethylene naphthalate FRPs to increase the compressive response of concrete. The authors also reported that the improvement in ultimate strain was roughly 10–15 times greater than the increase in compressive strength.

Table 3. Experimental compressive strength and ultimate strain.

Name of Specimen	Compressive Strength f_{cu}(MPa)	Enhancement in f_{cu}(%)	Ultimate Strain ϵ_{cu}	Enhancement in ϵ_{cu} (%)	Failure Mode
I-C	17.77	-	0.0022	-	-
I-1F	29.00	63.20	0.0590	2581.82	B
I-2F	35.80	101.48	0.0805	3559.10	A
I-3F	42.74	140.52	0.1010	4490.91	A
II-C	29.98	-	0.0030	-	-
II-1F	33.70	12.33	0.0401	1236.67	B
II-2F	36.80	22.67	0.0750	2400.00	B
II-3F	44.00	46.67	0.0820	2633.33	A
I-C	18.21	-	0.0020	-	-
I-1S	23.93	31.41	0.0203	915.00	B
I-2S	27.54	51.23	0.0550	2650.00	B
I-3S	33.60	84.51	0.0785	3825.00	A
II-C	28.87	-	0.0025	-	-
II-1S	34.11	18.15	0.0260	940.00	B
II-2S	36.02	24.77	0.0307	1128.00	B
II-3S	42.20	46.18	0.0430	1620.00	B

3.4. Impact of the Confinement Type

The comparison of improvement in compressive strength and ultimate strain are illustrated in Figures 10 and 11, respectively. The comparison is made for Type I and II RAC separately. Figure 10a demonstrates that the full wrap pattern enhanced the ultimate strength by 56%, 50%, and 32% more than the strip pattern for 1, 2, and 3 layers, respectively. For specimens with Type II RAC, the difference was marginal. An analogous trend was noted in the ultimate strain improvement. As illustrated in Figure 11a, the full wrap pattern outperformed the strip pattern by 666%, 909%, and 1667% for 1, 2, and 3 wraps, respectively. For higher unstrengthen strength, this contrast was 1013%, 1272%, and 297% for 1, 2, and 3 layers, respectively.

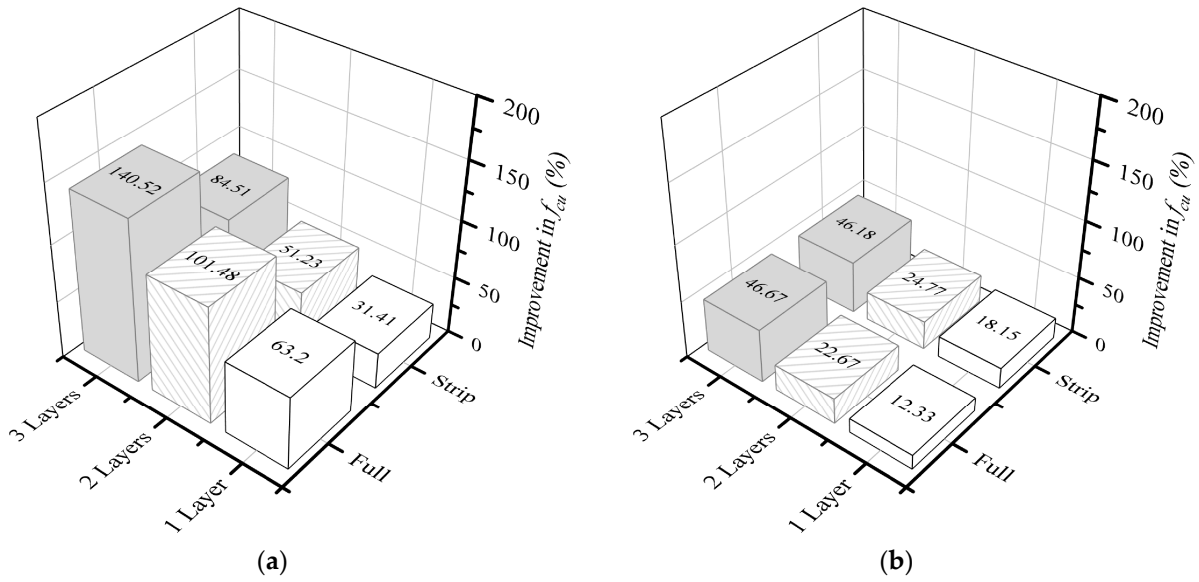

Figure 10. Analysis of compressive strength improvements attained using full and strip cotton FRP patterns for (**a**) low and (**b**) high unstrengthen strength samples.

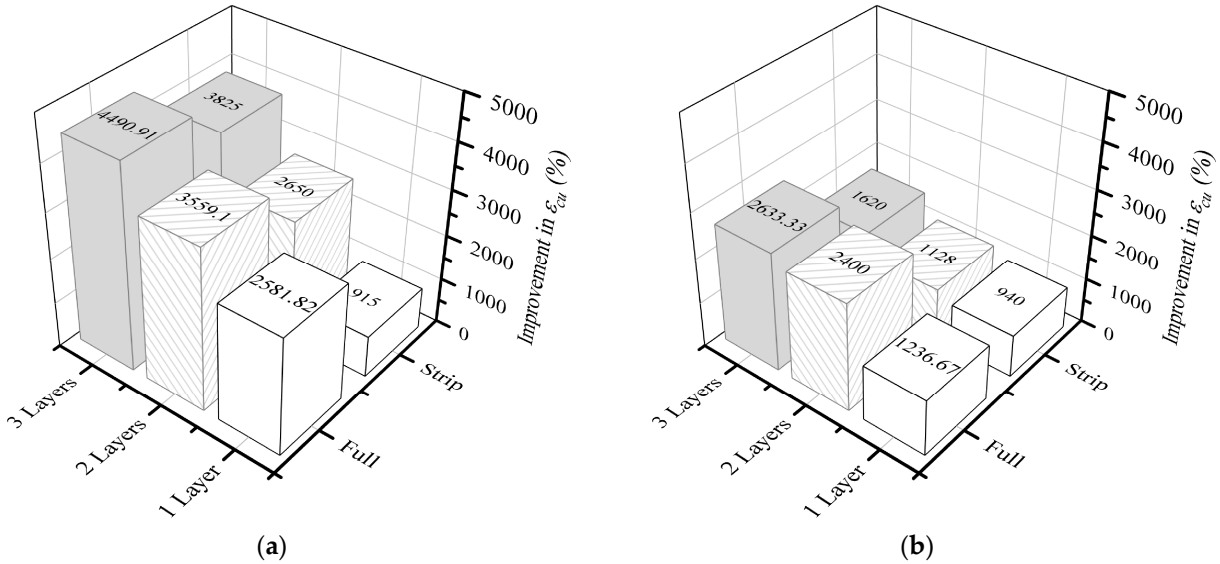

Figure 11. Analysis of compressive strain improvements attained using full and strip cotton FRP patterns for (**a**) low and (**b**) high unconfined strength specimens.

3.5. Impact of the Confinement Ratio

The confinement ratio, as previously defined, is usually employed as a key factor to measure the effectiveness of external confinement [74]. The unstrengthened strength negatively impacts the effectiveness of confinement [75]. The confinement effectiveness is typically improved by increasing the confinement magnitude [76]. Hence, the confinement ratio accounts for both parameters, providing a holistic assessment of confinement effectiveness. For the strip configuration, the confinement efficiency was observed to diminish. This reduction in efficiency was quantified using the method proposed by Mander et al. [77]. This approach assumes that the unconfined regions among the strip levels form 45° parabolas, as illustrated in Figure 12. The confinement efficiency factor, k_e, is then employed to the calculated confining pressure f_l in determining the effective confining pressure f_{le}, leading to Equation (1).

$$f_{le} = k_e f_l \tag{1}$$

The calculation of f_l was performed by assuming the equilibrium among the outward stresses exerted by the concrete core and the resulting hoop stresses in the CR confinement.

$$f_l = \frac{2n_c t_c f_t}{d_c} \tag{2}$$

where n_c, t_c, and f_t are the quantity, diameter, and fracture capacity of CR, respectively. The expression d_c shows the diameter of the cylinder. Following the suggestions of Mander et al. [77], the term k_e is calculated as the ratio of the unconfined regions A_{ie} shown in Figure 12 to the efficiently confined regions A_e, expressed as follows:

$$k_e = \frac{A_{ie}}{A_e} = \frac{\frac{\pi}{4} d_c^2 \left(1 - \frac{s'}{2d_c}\right)^2}{\frac{\pi d_c^2}{4}} \tag{3}$$

where s' denotes the clear spacing of two CR strips.

In this work, the confinement ratio ranged from 0.10 to 0.70. Figure 13a illustrates the impact of the confinement ratio on f_{cu} normalized by the unconfined strength f_{co}. It is clear that the compressive strength of CR-confined concrete was enhanced with a

confinement ratio increase, as depicted by the strong relationship in Figure 13a. The strain at the end of the initial parabolic part ϵ_{cc} is connected to the confinement ratio in Figure 13b. It is seen that ϵ_{cc} also improved with the confinement ratio, whereas this improvement showed a parabolically increasing trend. The stress corresponding to ϵ_{cc} is crucial to model Type A failure. Four specimens demonstrated Type A failure, as shown in Table 3. The corresponding f_{cc} values are plotted against the corresponding confinement ratios in Figure 13c, depicting an increasing trend. The stiffness of the second part Z, as observed in Figure 9, is an important parameter to explain the shape of the stress vs. strain graph of CR-confined RAC. A positive Z results in an ascending branch, as shown in Figure 13d. It is noted that the confinement ratio must at least be 0.40 to produce an increasing second part in the compressive stress vs. strain behavior of CR-confined RAC.

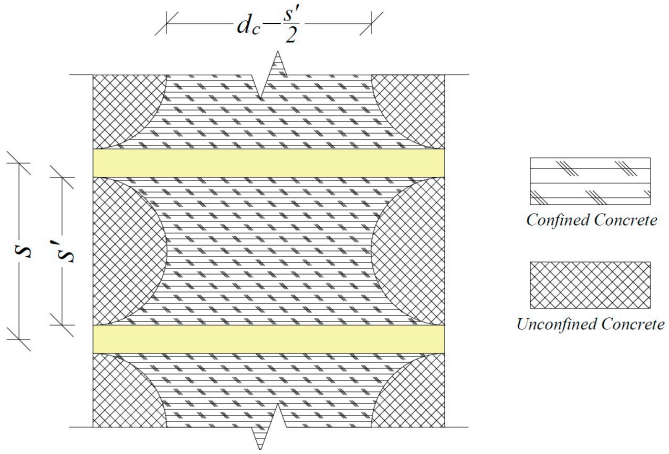

Figure 12. Graphical demonstration of the confined and unconfined areas along the height of concrete specimens.

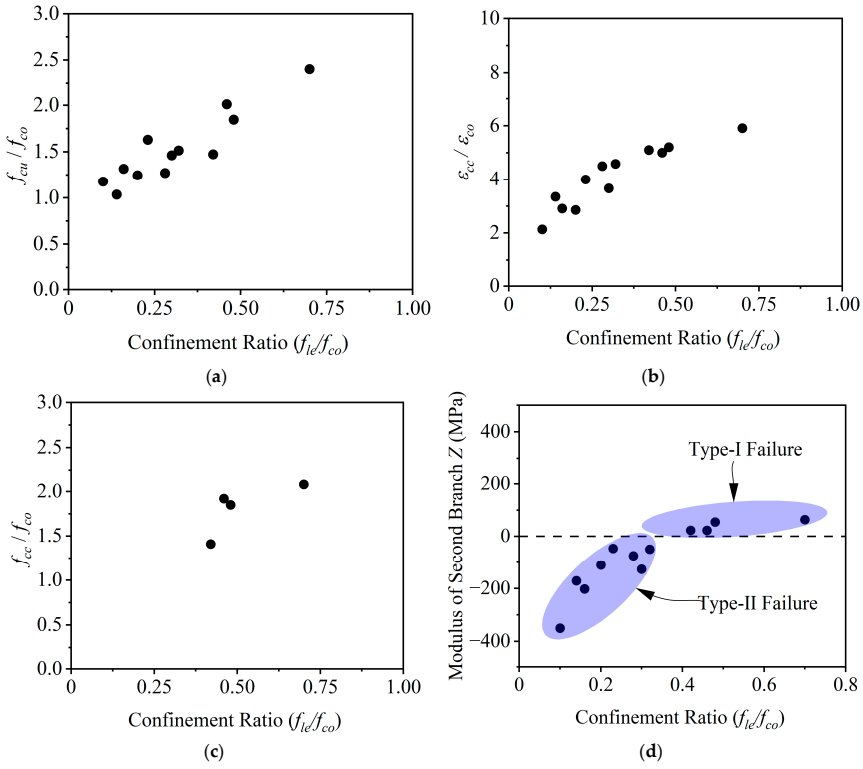

Figure 13. Impact of the confinement ratio on (**a**) normalized f_{cu}, (**b**) normalized ϵ_{cc}, (**c**) normalized f_{cc}, and (**d**) modulus of the second part.

4. Modeling of Stress vs. Strain Response

This section presents equations to find the compressive strength, ultimate strain, and key locations on the stress vs. strain response for CR-confined concrete. Earlier studies have determined that enhancements in both strength and strain may be primarily described as a function of the confinement ratio which is utilized to estimate the compressive stress vs. strain response of CR-confined concrete until failure. Due to the distinct properties of cotton, a new method is required to model the confinement mechanics, as conventional FRP expressions are unsuitable because of the substantial difference in the CR modulus compared to conventional FRP materials. The confinement ratio shows a pronounced impact on the stiffness of the second branch of the response, as illustrated in Figure 13d. Accurately predicting the slope of this second branch is crucial for modeling the full stress vs. strain curve until failure. The experimental data revealed that the confinement ratio is a key thing influencing this stiffness. Moreover, the experimental stress vs. strain behavior indicated that the first modulus remained unchanged after the cotton confinement was applied, which aligns with expectations since cotton confinement is passive and only activates with significant lateral expansion. As a result, cotton ropes have minimal impact under low axial deformation. In Figure 9, the points f_{cc}, ϵ_{cc}, f_{cu}, and Z need to be determined. After evaluating multiple existent formulations, it was concluded that the expression suggested by Popovics [78] provides the best fit for predicting these parameters. According to Popovics [78], the stress is computed as a function of various parameters, as follows:

$$f_c = f_{cc}\left[\frac{k\left(\frac{\epsilon_c}{\epsilon_{cc}}\right)}{k-1+\left(\frac{\epsilon_c}{\epsilon_{cc}}\right)^k}\right] \quad for\ \epsilon_c \leq \epsilon_{cc} \tag{4}$$

where

$$k = \frac{E_c}{E_c - \frac{f_{cc}}{\epsilon_{cc}}} \tag{5}$$

It is noteworthy that the curvature of the initial elastic part is handled by the parameter k. In this work, the elastic stiffness of the stress vs. strain curves was computed as 0.80 times $4700\sqrt{f_{co}}$ (MPa), whereas $4700\sqrt{f_{co}}$ is the recommendation by ACI 318 [79]. In Figure 14, the initial modulus of experimental curves is compared with the recommended value of ACI 318. Approximately a 20% reduction in elastic modulus was noted. Therefore, a factor of 0.80 was applied to the recommended value of ACI 318-19.

The second branch of the response was assumed to be linear, i.e., controlled by the slope parameter Z. The following sections present a nonlinear regression analysis of various experimental parameters and their corresponding regression equations. The Gauss–Newton algorithm was adopted for the nonlinear regression analysis. It is noted that failure Type A and Type B were approached slightly differently in analytical modeling. This is because the compressive strength f_{cu} and the stress at the termination of the initial parabolic part, i.e., f_{cc}, were concurrent in Type B failure. But these two parameters were different in the case of Type A failure. The flowchart to completely trace the stress vs. strain behavior of CR-confined concrete is demonstrated in Figure 15.

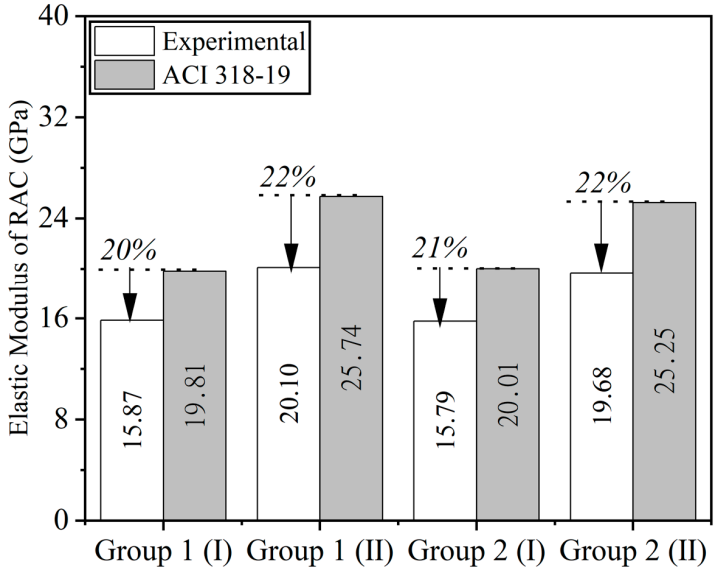

Figure 14. Comparison of the elastic modulus of RAC with the ACI 318-19 [79] recommended value.

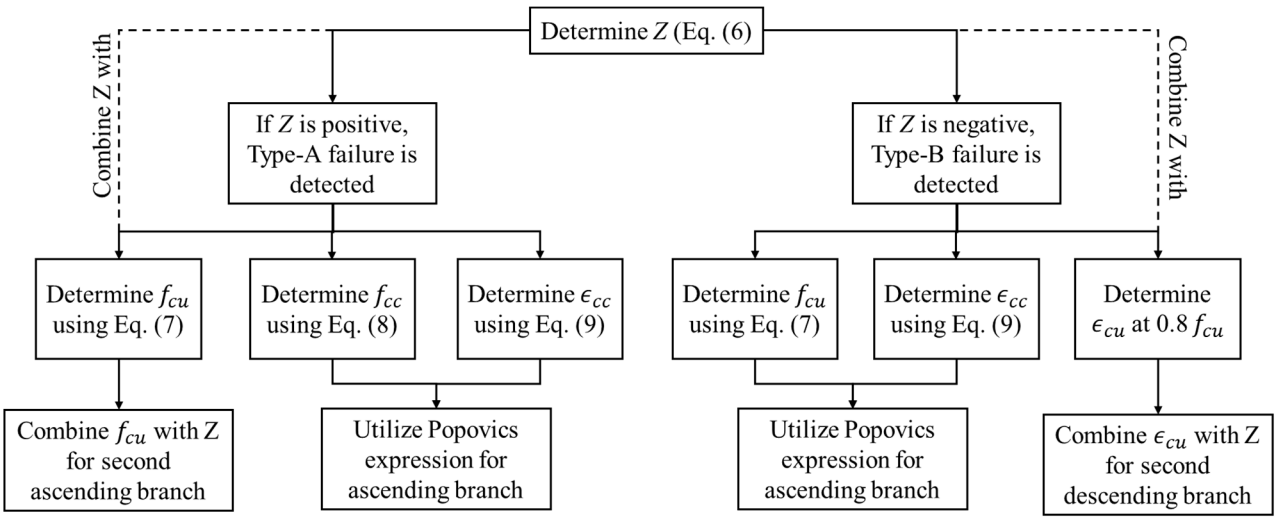

Figure 15. Flowchart to model the stress vs. strain behavior of CR-confined concrete.

4.1. Regression on Second Branch Z

As shown in Figure 15, the determination of the modulus of the second part of the stress vs. strain behavior of CR-confined concrete is of utmost importance. As illustrated in Figure 13d, this modulus was significantly affected by the confinement ratio. Nonlinear regression analysis was carried out on the experimental Z results, as reported in Figure 13d, resulting in Equation (6).

$$Z\ (MPa) = f_{co}^{0.414}\left[-21010.976 + 21058.708 \times \left(\frac{f_l}{f_{co}}\right)^{0.003}\right] \quad (6)$$

The R^2 value of Equation (6) was reported at 0.93, showing a good relationship with the experimental data. The comparison of predicted vs. experimental Z values is illustrated in Figure 16a.

4.2. Regression on the Compressive Strength

Figure 13a shows that the compressive strength of CR-confined was mainly subjected to the confinement ratio. Therefore, a regression analysis on the experimental compressive

strength values was performed by using the confinement ratio as the primary explanatory variable, resulting in Equation (7).

$$f_{cu} = 3.599 \times f_{co}^{0.629} \left[1 + 1.489 \left(\frac{f_l}{f_{co}} \right)^{1.315} \right] \quad (7)$$

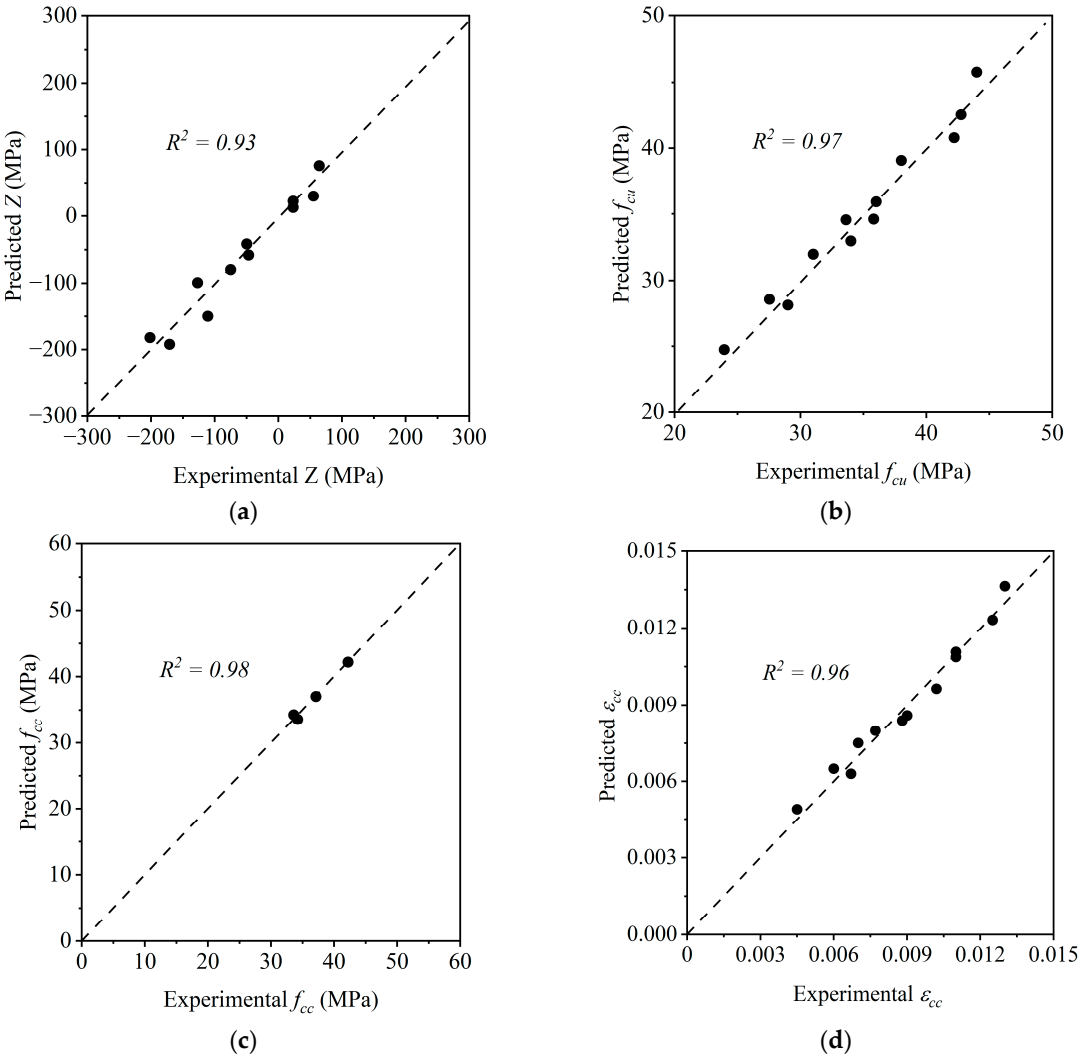

Figure 16. Analysis of experimental and predicted results of (**a**) the stiffness Z, (**b**) the compressive strength f_{cu}, (**c**) the stress f_{cc}, and (**d**) the strain ϵ_{cc}.

The R^2 value of Equation (7) was reported at 0.97, showing a good connection with the experimental data. The comparison of predicted vs. experimental f_{cu}values is indicated in Figure 16b.

4.3. Regression on the Stress f_{cc}

The stress f_{cc} is crucial in determining the termination point of the initial parabolic part in the case of Type A failure. Based on observations made in Figure 13c, the confinement ratio was again taken as an independent variable to propose an equation for predicting the stress f_{cc}. Based on nonlinear regression analysis, Equation (8) was proposed. The R^2 value of Equation (8) was 0.98, showing an excellent correlation with the experimental data (see Figure 16c).

$$f_{cc} = f_{co}^{0.479} \left[1 + 9.147 \left(\frac{f_l}{f_{co}} \right)^{0.261} \right] \quad (8)$$

4.4. Regression on the Strain ϵ_{cc}

The strain ϵ_{cc} is crucial for identifying the endpoint of the initial parabolic part of each of the Type A and Type B failures, as illustrated in Figure 15. Using nonlinear regression analysis, Equation (9) provided a reliable estimate for this value.

$$\epsilon_{cc} = \epsilon_{co}\left[1 + 6.451\left(\frac{f_l}{f_{co}}\right)^{0.605}\right] \tag{9}$$

The R^2 estimates of the modeled Equation (9) is 0.96, and its effectiveness is explicitly shown in Figure 16d. This demonstrates that the proposed model successfully accounts for over 96% of the variation observed in experimental results. Notably, the unconfined strain can be assumed to be 0.002 in the aforementioned expressions.

4.5. Similarity Between Predicted and Experimental Curves

The method outlined in Figure 15 was implemented, and the resulting predictions are illustrated in Figure 17. For Type B failure, the model forecasts indicated up to a 20% decrease in the compressive strength. The predictions demonstrated that the proposed method accurately captures the behavior of CR-confined concrete, providing a reasonable match with the experimental outcomes. Key parameters, such as the initial stiffness, compressive strength for each failure mode, ultimate strain values, and the second ascending and descending parts of the stress vs. strain curve, align closely with the experimental data, confirming the reliability of the approach.

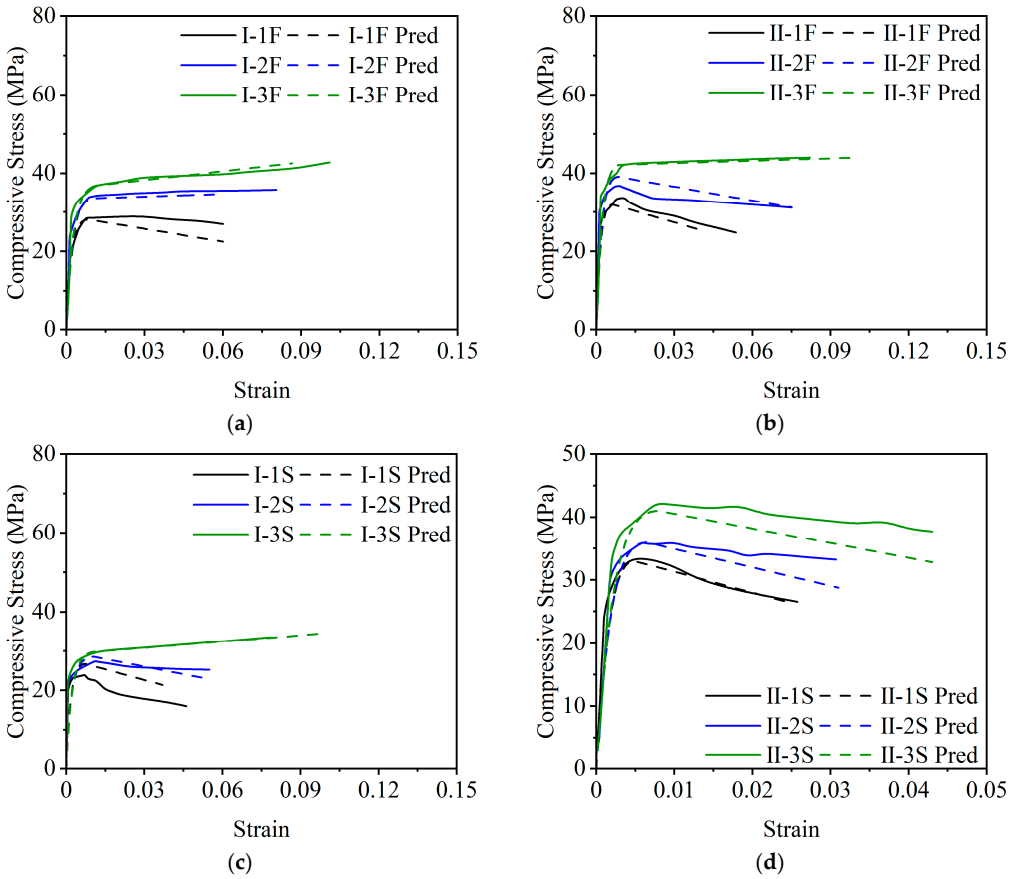

Figure 17. Comparison of the experimental and predicted compressive response of CR-confined RAC for (**a**) Group 1 specimens (Type I concrete), (**b**) Group 1 specimens (Type II concrete), (**c**) Group 2 specimens (Type I concrete), and (**d**) Group 2 specimens (Type II concrete).

5. Application of Neural Networks

Neural Networks (NNs) are one of the broadly utilized approaches in the domain of artificial intelligence [80]. NNs were utilized in this study for their capability to model complex non-linear relationships within these data. They have demonstrated potential in various structural engineering applications. While neural networks demand substantial computational resources and tend to be less interpretable than tree-based models, their adaptability makes them ideal for forecasting the compressive strength of CR-confined concrete. This study incorporated a neural network model to explore how deep learning techniques performed in comparison to traditional regression analysis using NNs.

In an artificial neural network, a neuron processing unit can symbolize several entities, like features, letters, concepts, or abstract configurations. These units are divided into input, output, and hidden units. The input units gather signals and data from the external environment [81], while the output units provide the processed results of the system. Hidden units, situated between input and output layers, are not directly observable outside the network [82]. Connection weights between neurons indicate the strength of interactions between them, encapsulating the depiction and handling of information.

An artificial neural network is an adaptive, non-programmatic, brain-inspired information processing system. It functions through transformations and dynamic behaviors within a parallel distributed network. This design partially mimics the human brain and nervous system's information processing at varying levels [83]. Neural networks find application across neuroscience, cognitive science, artificial intelligence, computer science, and other interdisciplinary fields.

Previously, machine learning was vastly utilized in civil engineering works [84–89]. In this study, the database for training the model was adopted from Talpur et al. [90]. In this study, the NN model was also employed to forecast the compressive strength of CR-strengthened concrete. A dataset of 142 concrete samples strengthened with natural fibers sourced from existing works was used for this purpose. The compressive strength of the confined concrete was correlated with factors such as the compressive strength of unconfined concrete, the magnitude and diameter of hemp ropes, and the specimen size. Additionally, the cross-sectional shape was found to influence the efficiency of external confinement. For rectangular cross-sections, the corner radius significantly affects the confinement efficiency. Consequently, the explanatory variables included the cross-sectional shape, rope thickness, rope tensile strength, and the strength of unconfined concrete. The dataset was categorized into training and testing sets with an 80% to 20% ratio. The Python programming language was used for the NN model. KERAS was used to build and train the model. PANDAS was used to read and preprocess the dataset. The number of layers was six. The NN model's predictions are shown in Figure 18. In Figure 18, only actual and predicted values of the current experimental program are shown. It is observed that the model predicted the compressive strength of fully wrapped specimens with reasonable accuracy, whereas the compressive strength of strip-wrapped specimens was overestimated. This can be ascribed to the scarcity of strip-wrapped specimens in the dataset utilized for training the model. Further, the height of the full-wrap cotton ropes was divided by the total height of partial-wrap cotton ropes to drive the strength reduction factor. The strength reduction factor of 0.67 was multiplied by predicted values. The findings are displayed in Figure 18c. It is observed that the model predicted the compressive strength of partially wrapped specimens with reasonable accuracy using the strength reduction factor. The model performance is given in Table 4.

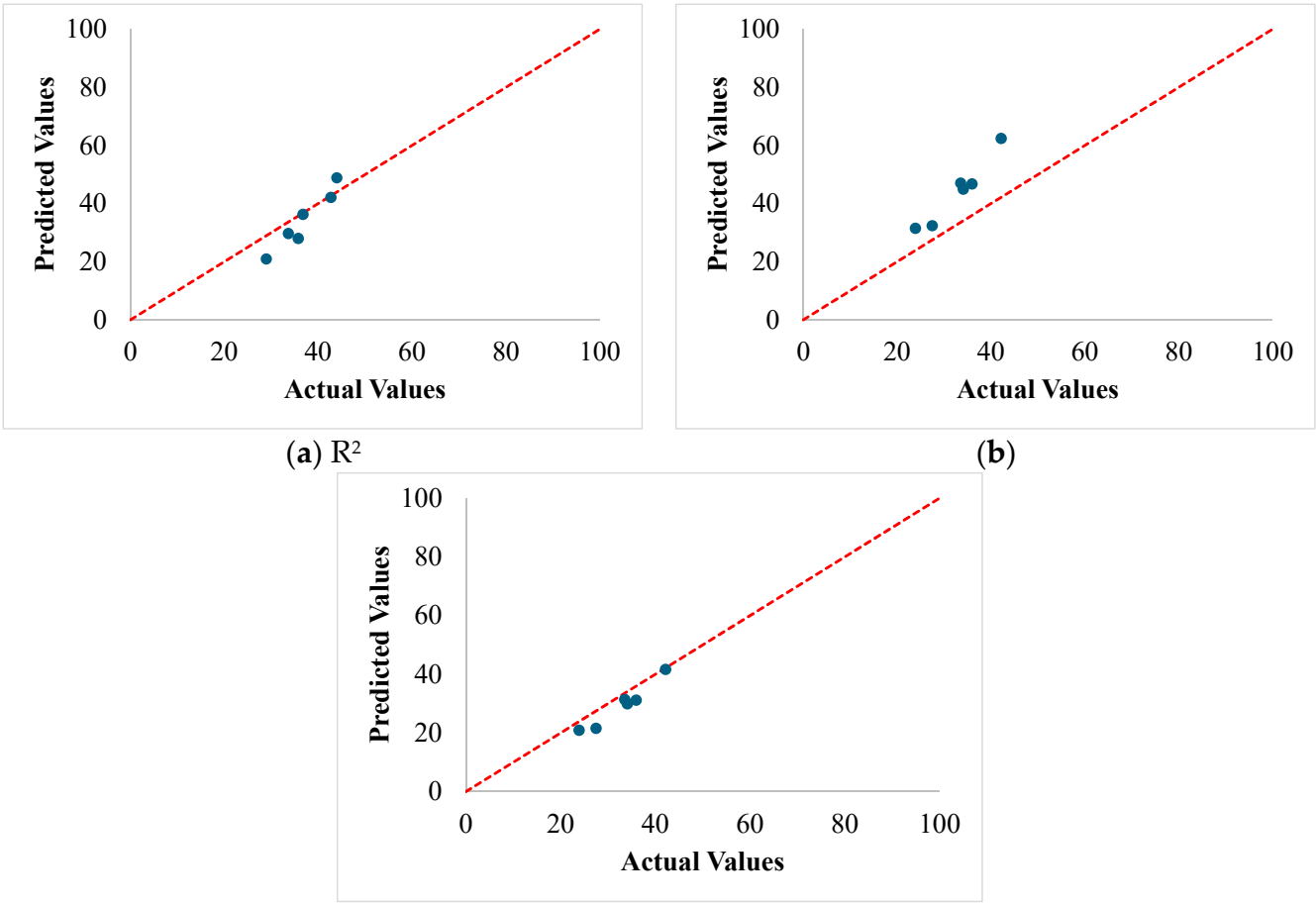

Figure 18. Comparison of NN-predicted and experimental compressive strength (**a**) full wrap, (**b**) strip wrap original, and (**c**) strip wrap factored.

Table 4. Performance of model.

	Full Wrap	Strip Wrap	Factored Strip Wrap
R^2 Square	0.931	0.951	0.951
Means square error (MSE)	27.83	149.96	15.10
Mean absolute error (MAE)	4.32	11.24	3.46

6. Future Research Directions

Since this is a preliminary work on CR-confined ReCA, factors like long-term durability were not considered. However, future works are directed to explore this perspective. The performance of CR-confined ReCA in different environmental conditions needs to be assessed. The fire resistance of CR-confined ReCA is another important aspect that needs attention in future research. The shear behavior of ReCA is inferior to natural aggregate concrete, attributed to the substandard compressive strength of ReCA. Various configurations of CR confinement to enhance the shear response of ReCA may be assessed. Importantly, it is noted in the Introduction that cotton ropes are significantly cheaper than synthetic FRPs. However, a life-cycle assessment of cotton ropes in comparison to that of synthetic FRPs needs to be performed in future studies.

To enhance the durability of cotton ropes in harsh conditions, treatments like water-proofing, UV-resistant coatings, and anti-microbial agents can protect against moisture, sunlight, and microbial growth. Impregnating with resins, adding polymer coatings, or blending with additives like linseed oil improves resistance while maintaining sustainabil-

ity. Physical protections, such as sheathing or hybridizing with synthetic fibers, and proper storage in dry areas further extend longevity, ensuring reliable performance in challenging environments. Such treatments should be investigated in future works.

The confinement ratio is defined as the ratio of the applied confinement pressure to the unconfined compressive strength of concrete. In real-world applications, the diameter is usually greater than the 150 mm adopted in this work. From Equation (2), the number of cotton ropes should be increased in proportion to the diameter of the real-world column to achieve a confinement ratio in excess of 0.40. However, future studies should extend this by examining the confinement efficiency of cotton ropes to large-scale columns, both in the form of full wraps and strips.

7. Conclusions

This study investigates the potential of cotton ropes (CRs) as a sustainable and cost-effective alternative to synthetic FRPs for concrete confinement. Cotton ropes offer environmental benefits, such as lower CO_2 emissions and reduced energy requirements, along with high rupture strain, making them suitable for structural strengthening. Despite these advantages, partial confinement using CR strips remains underexplored. To fill this gap, the research evaluated the effectiveness of CR strips for confining concrete, including when natural coarse aggregates were replaced with recycled concrete aggregates. The study also compared CR strip performance with the fully wrapped method and developed analytical expressions to forecast the structural effect of CRs on concrete.

1. The stress–strain curves showed an initially stiff, elastic response that followed either an ascending or descending second branch, based on the confinement level. Importantly, the slope of the second branch transitioned from negative to positive with the increment in the confinement ratio;
2. The improvements in compressive strength and ultimate strain varied notably among specimens. Specimen I-3F showed the highest compressive strength increase of 140.52%, while Specimen II-3F achieved 46.67%. Strip configurations for Type I RAC outperformed full wraps for Type II RAC, with Specimen I-3S showing an 84.51% improvement. Ultimate strain enhancements ranged from 915% to 4490.91%, attributed to the high rupture strain of the cotton rope confinement. These improvements were significantly influenced by the confinement ratio and unconfined compressive strength;
3. For Type I RAC, complete wrapping outperformed strip configurations in ultimate strength, with improvements of 56%, 50%, and 32% for 1, 2, and 3 layers, respectively. In contrast, Type II RAC showed marginal differences between the configurations. A similar trend was observed for ultimate strain, where complete wrapping surpassed strip configurations by 666%, 909%, and 1667% for 1, 2, and 3 layers. For higher unconfined strength, the differences were 1013%, 1272%, and 297% for 1, 2, and 3 layers. These results emphasize the superior performance of complete wrapping, especially for specimens with lower unconfined strength;
4. In this work, the confinement ratio ranged from 0.10 to 0.70, significantly influencing the compressive behavior of cotton rope-confined concrete. The compressive strength (f_{cu}), normalized by the unconfined strength (f_{co}), increased consistently with the confinement ratio, demonstrating a strong correlation. The strain at the end of the initial parabolic branch also improved with confinement, following a parabolic trend. The corresponding stress values showed a positive relationship with the confinement ratio. The results showed that a minimum confinement ratio of approximately 0.40 is necessary to achieve an ascending second branch in the compressive response of CR-confined RAC;

5. Popovics' formulation was used to model the initial parabolic branch of the stress vs. strain response for CR-confined RAC, revealing its elastic modulus to be about 20% lower than ACI 318-19 predictions. A linear approximation effectively captured the post-peak behavior based on the confinement ratio. Nonlinear regression developed expressions for key points on the compressive curve, achieving close agreement with experimental results;
6. In conclusion, this study demonstrated the potential of neural network models in forecasting the compressive strength of CR-confined concrete. While the model performed well for fully wrapped specimens, it underestimated the strength of strip-wrapped specimens due to a limited dataset. This highlights the need for future research to expand the database, particularly focusing on strip-wrapped configurations, to improve prediction accuracy and understanding of natural rope confinement. It is important to note that the findings of this work cannot be generalized to other natural confinements. This is because cotton ropes have large rupture strains, unlike hemp. Therefore, despite being passive in principle, the findings of this work should be limited to cotton rope confinement only.

Author Contributions: Conceptualization, K.R., A.E., H.W., P.S., W.K., Q.H. and C.B.; Methodology, P.J.; Formal Analysis, A.E.; Writing—original draft, K.R., A.E., H.W., P.S., P.J., W.K., Q.H. and C.B.; Writing—review and editing, K.R., A.E., H.W., P.S., P.J., W.K., Q.H. and C.B. All authors have read and agreed to the published version of the manuscript.

Funding: This research budget was allocated by the National Science, Research and Innovation Fund (NSRF) and King Mongkut's University of Technology, North Bangkok (Project no. KMUTNB-FF-67-B-36).

Data Availability Statement: The original contributions presented in this study are included in the article. Further inquiries can be directed to the corresponding author.

Acknowledgments: This research budget was allocated by the National Science, Research and Innovation Fund (NSRF) and King Mongkut's University of Technology, North Bangkok (Project no. KMUTNB-FF-67-B-36). Thanks are also extended to Asian Institute of Technology (AIT), Thailand, for supporting the test facilities.

Conflicts of Interest: The authors declare no conflicts of interest.

References

1. Poon, C.; Shui, Z.; Lam, L. Effect of microstructure of ITZ on compressive strength of concrete prepared with recycled aggregates. *Constr. Build. Mater.* **2004**, *18*, 461–468. [CrossRef]
2. Marinković, S.; Radonjanin, V.; Malešev, M.; Ignjatović, I. Comparative environmental assessment of natural and recycled aggregate concrete. *Waste Manag.* **2010**, *30*, 2255–2264. [CrossRef] [PubMed]
3. Zeng, Y.; Guo, H.; Lei, J.; Hu, Y.; Yang, Z. Study on the mechanical properties of recycled brick coarse aggregate concrete based on finite element modeling. *J. Build. Eng.* **2024**, *95*, 110110. [CrossRef]
4. Grdic, Z.J.; Toplicic-Curcic, G.A.; Despotovic, I.M.; Ristic, N.S. Properties of self-compacting concrete prepared with coarse recycled concrete aggregate. *Constr. Build. Mater.* **2010**, *24*, 1129–1133. [CrossRef]
5. Xu, X.; Luo, Y.; Sreeram, A.; Wu, Q.; Chen, G.; Cheng, S.; Chen, Z.; Chen, X. Potential use of recycled concrete aggregate (RCA) for sustainable asphalt pavements of the future: A state-of-the-art review. *J. Clean. Prod.* **2022**, *344*, 130893. [CrossRef]
6. Khan, M.; Rehman, A.; Ali, M. Efficiency of silica-fume content in plain and natural fiber reinforced concrete for concrete road. *Constr. Build. Mater.* **2020**, *244*, 118382. [CrossRef]
7. Wang, Z.; Zhang, Z.; Jin, X. A study on the spatial network characteristics and effects of CDW generation in China. *Waste Manag.* **2021**, *128*, 179–188. [CrossRef] [PubMed]
8. Galán, B.; Viguri, J.; Cifrian, E.; Dosal, E.; Andres, A. Influence of input streams on the construction and demolition waste (CDW) recycling performance of basic and advanced treatment plants. *J. Clean. Prod.* **2019**, *236*, 117523. [CrossRef]

9. Mak, T.M.; Chen, P.-C.; Wang, L.; Tsang, D.C.; Hsu, S.; Poon, C.S. A system dynamics approach to determine construction waste disposal charge in Hong Kong. *J. Clean. Prod.* **2019**, *241*, 118309. [CrossRef]
10. Mo, K.H.; Thomas, B.S.; Yap, S.P.; Abutaha, F.; Tan, C.G. Viability of agricultural wastes as substitute of natural aggregate in concrete: A review on the durability-related properties. *J. Clean. Prod.* **2020**, *275*, 123062. [CrossRef]
11. Wang, B.; Yan, L.; Fu, Q.; Kasal, B. A Comprehensive Review on Recycled Aggregate and Recycled Aggregate Concrete. *Resour. Conserv. Recycl.* **2021**, *171*, 105565. [CrossRef]
12. Yang, S.; Lim, Y. Mechanical strength and drying shrinkage properties of RCA concretes produced from old railway concrete sleepers using by a modified EMV method. *Constr. Build. Mater.* **2018**, *185*, 499–507. [CrossRef]
13. Pu, Y.; Li, L.; Wang, Q.; Shi, X.; Luan, C.; Zhang, G.; Fu, L.; El-Fatah Abomohra, A. Accelerated carbonation technology for enhanced treatment of recycled concrete aggregates: A state-of-the-art review. *Constr. Build. Mater.* **2021**, *282*, 122671. [CrossRef]
14. Zhang, K.; Xiao, J. Prediction model of carbonation depth for recycled aggregate concrete. *Cem. Concr. Compos.* **2018**, *88*, 86–99. [CrossRef]
15. Kleijer, A.; Lasvaux, S.; Citherlet, S.; Viviani, M. Product-specific Life Cycle Assessment of ready mix concrete: Comparison between a recycled and an ordinary concrete. *Resour. Conserv. Recycl.* **2017**, *122*, 210–218. [CrossRef]
16. Yazdanbakhsh, A.; Bank, L.C.; Baez, T.; Wernick, I. Comparative LCA of concrete with natural and recycled coarse aggregate in the New York City area. *Int. J. Life Cycle Assess.* **2018**, *23*, 1163–1173. [CrossRef]
17. Jin, R.; Chen, Q.; Soboyejo, A. Survey of the current status of sustainable concrete production in the U.S. *Resour. Conserv. Recycl.* **2015**, *105*, 148–159. [CrossRef]
18. Al-Bayati, H.K.A.; Das, P.K.; Tighe, S.L.; Baaj, H. Evaluation of various treatment methods for enhancing the physical and morphological properties of coarse recycled concrete aggregate. *Constr. Build. Mater.* **2016**, *112*, 284–298. [CrossRef]
19. Katz, A. Properties of concrete made with recycled aggregate from partially hydrated old concrete. *Cem. Concr. Res.* **2003**, *33*, 703–711. [CrossRef]
20. Mohajerani, A.; Vajna, J.; Cheung, T.H.H.; Kurmus, H.; Arulrajah, A.; Horpibulsuk, S. Practical recycling applications of crushed waste glass in construction materials: A review. *Constr. Build. Mater.* **2017**, *156*, 443–467. [CrossRef]
21. Singh, L.P.; Bisht, V.; Aswathy, M.S.; Chaurasia, L.; Gupta, S. Studies on performance enhancement of recycled aggregate by incorporating bio and nano materials. *Constr. Build. Mater.* **2018**, *181*, 217–226. [CrossRef]
22. Bru, K.; Touzé, S.; Bourgeois, F.; Lippiatt, N.; Ménard, Y. Assessment of a microwave-assisted recycling process for the recovery of high-quality aggregates from concrete waste. *Int. J. Miner. Process.* **2014**, *126*, 90–98. [CrossRef]
23. Ismail, S.; Ramli, M. Mechanical strength and drying shrinkage properties of concrete containing treated coarse recycled concrete aggregates. *Constr. Build. Mater.* **2014**, *68*, 726–739. [CrossRef]
24. Katz, A. Treatments for the Improvement of Recycled Aggregate. *J. Mater. Civ. Eng.* **2004**, *16*, 597–603. [CrossRef]
25. Li, Y.-G.; Liang, H.-H.; Bai, S.-L.; Zhou, Y.; Sun, G.; Su, Y.-R.; Gao, A.-L.; Zhang, D.-L.; Li, S.-P. Molecular Characterization and Variation of the Celiac Disease Epitope Domains among α-Gliadin Genes in *Aegilops tauschii*. *J. Agric. Food Chem.* **2017**, *65*, 3422–3429. [CrossRef]
26. Wang, L.; Wang, J.; Qian, X.; Chen, P.; Xu, Y.; Guo, J. An environmentally friendly method to improve the quality of recycled concrete aggregates. *Constr. Build. Mater.* **2017**, *144*, 432–441. [CrossRef]
27. Liu, Z.; Chin, C.S.; Xia, J. Improving recycled coarse aggregate (RCA) and recycled coarse aggregate concrete (RCAC) by biological denitrification phenomenon. *Constr. Build. Mater.* **2021**, *301*, 124338. [CrossRef]
28. Gao, C.; Huang, L.; Yan, L.; Jin, R.; Kasal, B. Strength and ductility improvement of recycled aggregate concrete by polyester FRP-PVC tube confinement. *Compos. Part B Eng.* **2019**, *162*, 178–197. [CrossRef]
29. Haroun, M.A.; Elsanadedy, H.M. Fiber-Reinforced Plastic Jackets for Ductility Enhancement of Reinforced Concrete Bridge Columns with Poor Lap-Splice Detailing. *J. Bridg. Eng.* **2005**, *10*, 749–757. [CrossRef]
30. Wang, W.; Sheikh, M.N.; Al-Baali, A.Q.; Hadi, M.N. Compressive behaviour of partially FRP confined concrete: Experimental observations and assessment of the stress-strain models. *Constr. Build. Mater.* **2018**, *192*, 785–797. [CrossRef]
31. Castillo, E.d.R.; Griffith, M.; Ingham, J. Seismic behavior of RC columns flexurally strengthened with FRP sheets and FRP anchors. *Compos. Struct.* **2018**, *203*, 382–395. [CrossRef]
32. Dong, J.; Wang, Q.; He, D.; Guan, Z. CFRP sheets for flexural strengthening of RC beams. In Proceedings of the 2011 International Conference on Multimedia Technology (ICMT), Hangzhou, China, 26–28 July 2011; pp. 1000–1003.
33. Ali, O.K.; Al-Hadithi, A.I.; Noaman, A.T. Flexural performance of layered PET fiber reinforced concrete beams. *Structures* **2022**, *35*, 55–67. [CrossRef]
34. Erfan, A.M.; Elnaby, R.M.A.; Badr, A.A.; El-Sayed, T.A. Flexural behavior of HSC one way slabs reinforced with basalt FRP bars. *Case Stud. Constr. Mater.* **2021**, *14*, e00513. [CrossRef]

35. Attari, N.; Amziane, S.; Chemrouk, M. Flexural strengthening of concrete beams using CFRP, GFRP and hybrid FRP sheets. *Constr. Build. Mater.* **2012**, *37*, 746–757. [CrossRef]
36. Song, B.; Jin, L.; Zhang, J.; Du, X. Size effect tests on shear strength of Basalt FRP-RC deep beams with different shear-span ratios. *Eng. Struct.* **2023**, *294*, 116740. [CrossRef]
37. Farghaly, A.S. Benmokrane, BShear behavior of FRP-reinforced concrete deep beams without web reinforcement. *J. Compos. Constr.* **2013**, *17*, 04013015. [CrossRef]
38. Chen, J.; Teng, J. Shear capacity of FRP-strengthened RC beams: FRP debonding. *Constr. Build. Mater.* **2003**, *17*, 27–41. [CrossRef]
39. Baggio, D.; Soudki, K.; Noël, M. Strengthening of shear critical RC beams with various FRP systems. *Constr. Build. Mater.* **2014**, *66*, 634–644. [CrossRef]
40. Bousias, S.; Spathis, A.; Fardis, M. Seismic retrofitting of columns with lap-splices through CFRP jackets. In Proceedings of the 13th World Conference on Earthquake Engineering, Vancouver, BC, Canada, 1–6 August 2004.
41. Bournas, D.A.; Triantafillou, T.C. Bond Strength of Lap-Spliced Bars in Concrete Confined with Composite Jackets. *J. Compos. Constr.* **2011**, *15*, 156–167. [CrossRef]
42. Ghosh, K.K.; Sheikh, S.A. Seismic Upgrade with Carbon Fiber-Reinforced Polymer of Columns Containing Lap-Spliced Reinforcing Bars. *ACI Struct. J.* **2007**, *104*, 227–236. [CrossRef]
43. ElGawady, M.; Endeshaw, M.; McLean, D.; Sack, R. Retrofitting of Rectangular Columns with Deficient Lap Splices. *J. Compos. Constr.* **2009**, *14*, 22–35. [CrossRef]
44. Harries, K.; Ricles, J.; Pissiki, S.; Sause, R. Seismic Retrofit of Lap Splices in Nonductile Columns Using CFRP Jackets. *ACI Struct. J.* **2006**, *103*, 226–236. [CrossRef]
45. Jamatia, R.; Deb, A. Size Effect in FRP-Confined Concrete under Axial Compression. *J. Compos. Constr.* **2017**, *21*, 04017045. [CrossRef]
46. Rousakis, T.C.; Karabinis, A.I.; Kiousis, P.D. FRP-confined concrete members: Axial compression experiments and plasticity modelling. *Eng. Struct.* **2007**, *29*, 1343–1353. [CrossRef]
47. Jiang, T.; Wang, X.M.; Zhang, W.P.; Chen, G.M.; Lin, Z.H. Behavior of FRP-Confined Recycled Brick Aggregate Concrete under Monotonic Compression. *J. Compos. Constr.* **2020**, *24*, 04020067. [CrossRef]
48. Zeng, J.-J.; Guo, Y.-C.; Gao, W.-Y.; Li, J.-Z.; Xie, J.-H. Behavior of Partially and Fully FRP-Confined Circularized Square Columns under Axial Compression. *Constr. Build. Mater.* **2017**, *152*, 319–332. [CrossRef]
49. Lim, J.C.; Ozbakkaloglu, T. Confinement Model for FRP-Confined High-Strength Concrete. *J. Compos. Constr.* **2014**, *18*, 04013058. [CrossRef]
50. Ozbakkaloglu, T.; Lim, J.C.; Vincent, T. FRP-confined concrete in circular sections: Review and assessment of stress–strain models. *Eng. Struct.* **2013**, *49*, 1068–1088. [CrossRef]
51. Yoddumrong, P.; Rodsin, K.; Katawaethwarag, S. Seismic Strengthening of Low-Strength RC Concrete Columns using Low-Cost Glass Fiber Reinforced Polymers (GFRPs). *Case Stud. Constr. Mater.* **2020**, *13*, e00383. [CrossRef]
52. Sen, T.; Reddy, H.J. Efficacy of bio derived jute FRP composite based technique for shear strength retrofitting of reinforced concrete beams and its comparative analysis with carbon and glass FRP shear retrofitting schemes. *Sustain. Cities Soc.* **2014**, *13*, 105–124. [CrossRef]
53. Haufe, J.; Carus, M. *Hemp Fibres for Green Products–An Assessment of Life Cycle Studies on Hemp Fibre Applications*; European Industrial Hemp Association (EIHA): Wolfsburg, Germany, 2011.
54. De Beus, N.; Carus, N.; Barth, M. *Carbon Footprint and Sustainability of Different Natural Fibres for Biocomposites and Insulation Material*; nova-Institut GmbH: Hürth, Germany, 2019.
55. Zwawi, M. A Review on Natural Fiber Bio-Composites, Surface Modifications and Applications. *Molecules* **2021**, *26*, 404. [CrossRef]
56. Ivanova, I.; Assih, J.; Dontchev, D. Investigation of the mechanical behavior of natural vegetable fibers used in composite materials for structural strengthening. *Key Eng. Mater.* **2021**, *888*, 15–21. [CrossRef]
57. Yang, K.; Wang, H.; Liu, Z. Evaluation on mechanical properties of high-performance biocomposite bridge deck structure: A review. *Polym. Compos.* **2021**, *42*, 6265–6297. [CrossRef]
58. Ekundayo, G. Reviewing the Development of Natural Fiber Polymer Composite: A Case Study of Sisal and Jute. *Am. J. Mech. Mater. Eng.* **2019**, *3*, 1–10. [CrossRef]
59. Rajak, D.K.; Wagh, P.H.; Linul, E. Manufacturing technologies of carbon/glass fiber-reinforced polymer composites and their properties: A review. *Polymers* **2021**, *13*, 3721. [CrossRef] [PubMed]
60. Bai, Y.-L.; Dai, J.-G.; Teng, J.G. Cyclic Compressive Behavior of Concrete Confined with Large Rupture Strain FRP Composites. *J. Compos. Constr.* **2013**, *18*, 04013025. [CrossRef]
61. Dai, J.-G.; Lam, L.; Ueda, T. Seismic retrofit of square RC columns with polyethylene terephthalate (PET) fibre reinforced polymer composites. *Constr. Build. Mater.* **2012**, *27*, 206–217. [CrossRef]

62. Saleem, S.; Hussain, Q.; Pimanmas, A. Compressive Behavior of PET FRP–Confined Circular, Square, and Rectangular Concrete Columns. *J. Compos. Constr.* **2016**, *21*, 04016097. [CrossRef]
63. Han, Q.; Yuan, W.; Bai, Y.; Du, X. Compressive behavior of large rupture strain (LRS) FRP-confined square concrete columns: Experimental study and model evaluation. *Mater. Struct.* **2020**, *53*, 99. [CrossRef]
64. Yuan, W.-Y.; Han, Q.; Bai, Y.-L.; Du, X.-L.; Yan, Z.-W. Compressive behavior and modelling of engineered cementitious composite (ECC) confined with LRS FRP and conventional FRP. *Compos. Struct.* **2021**, *272*, 114200. [CrossRef]
65. Pham, T.M.; Hadi, M.N.S.; Youssef, J. Optimized FRP Wrapping Schemes for Circular Concrete Columns under Axial Compression. *J. Compos. Constr.* **2015**, *19*, 04015015. [CrossRef]
66. Triantafyllou, G.G.; Rousakis, T.C.; Karabinis, A.I. Axially Loaded Reinforced Concrete Columns with a Square Section Partially Confined by Light GFRP Straps. *J. Compos. Constr.* **2015**, *19*, 04014035. [CrossRef]
67. Wei, H.; Wu, Z.; Guo, X.; Yi, F. Experimental study on partially deteriorated strength concrete columns confined with CFRP. *Eng. Struct.* **2009**, *31*, 2495–2505. [CrossRef]
68. *ASTM D3013-13*; Standard Specification for Epoxy Molding Compounds. ASTM International: West Conshohocken, PA, USA, 2021. Available online: https://www.astm.org/d3013-13.html (accessed on 30 April 2022).
69. *ACI SPEC-440.12-22*; Strengthening of Concrete Structures with Externally Bonded Fiber-Reinforced Polymer (FRP) Materials Using the Wet Layup Method—Specification. ASTM International: West Conshohocken, PA, USA, 2022.
70. Zeng, J.-J.; Duan, Z.-J.; Guo, Y.-C.; Xie, Z.-H.; Li, L.-J. Novel fiber-reinforced polymer cross wrapping strengthening technique: A comparative study. *Adv. Struct. Eng.* **2019**, *23*, 979–996. [CrossRef]
71. Zeng, J.-J.; Guo, Y.-C.; Gao, W.-Y.; Chen, W.-P.; Li, L.-J. Stress-strain behavior of concrete in circular concrete columns partially wrapped with FRP strips. *Compos. Struct.* **2018**, *200*, 810–828. [CrossRef]
72. Vu, X.H.; Malecot, Y.; Daudeville, L.; Buzaud, E. Experimental analysis of concrete behavior under high confinement: Effect of the saturation ratio. *Int. J. Solids Struct.* **2009**, *46*, 1105–1120. [CrossRef]
73. Yuan, W.-Y.; Bai, Y.-L.; Han, Q.; Zhang, S.-M. Large Rupture Strain FRP-Confined Concrete Columns of Different Sizes: Experiments and Stress–Strain Models. *J. Compos. Constr.* **2022**, *26*, 04022040. [CrossRef]
74. Cusson, D.; Paultre, P. Stress-Strain Model for Confined High-Strength Concrete. *J. Struct. Eng.* **1995**, *121*, 468–477. [CrossRef]
75. Mandal, S.; Hoskin, A.; Fam, A. Influence of Concrete Strength on Confinement Effectiveness of Fiber-Reinforced Polymer Circular Jackets. *ACI Struct. J.* **2005**, *102*, 383–392. [CrossRef]
76. Bai, Y.-L.; Liu, S.-Z.; Mei, S.-J. Compressive behavior and modeling of concrete wrapped by hybrid low-high elongation capacities FRP. *Eng. Struct.* **2024**, *300*, 117155. [CrossRef]
77. Mander, J.B.; Priestley, M.J.N.; Park, R. Theoretical Stress-Strain Model for Confined Concrete. *J. Struct. Eng.* **1988**, *114*, 1804–1826. [CrossRef]
78. Popovics, S. A Numerical Approach to the Complete Stress-Strain Curve of Concrete. *Cem. Concr. Res.* **1973**, *3*, 583–599. [CrossRef]
79. *ACI 318-19*; Building Code Requirements for Structural Concrete and Commentary. American Concrete Institute: Indianapolis, IN, USA, 2019.
80. Azadeh, A.; Seif, J.; Sheikhalishahi, M.; Yazdani, M. An integrated support vector regression–imperialist competitive algorithm for reliability estimation of a shearing machine. *Int. J. Comput. Integr. Manuf.* **2016**, *29*, 16–24. [CrossRef]
81. Balcazar, J.; Gavalda, R.; Siegelmann, H. Computational power of neural networks: A characterization in terms of Kolmogorov complexity. *IEEE Trans. Inf. Theory* **1997**, *43*, 1175–1183. [CrossRef]
82. Bauer, M.; Martienssen, W. Lyapunov exponents and dimensions of chaotic neural networks. *J. Phys. A Math. Gen.* **1991**, *24*, 4557–4566. [CrossRef]
83. Kasabov, N.; Scott, N.M.; Tu, E.; Marks, S.; Sengupta, N.; Capecci, E.; Othman, M.; Doborjeh, M.G.; Murli, N.; Hartono, R.; et al. Evolving spatio-temporal data machines based on the NeuCube neuromorphic framework: Design methodology and selected applications. *Neural Networks* **2016**, *78*, 1–14. [CrossRef] [PubMed]
84. Fakhrian, S.; Behbahani, H.; Mashhadi, S. Predicting Post-Fire Behavior of Green Geopolymer Mortar Containing Recycled Concrete Aggregate via GEP Approach. *J. Soft Comput. Civ. Eng.* **2020**, *4*, 22–45. [CrossRef]
85. Chen, L.; Nouri, Y.; Allahyarsharahi, N.; Naderpour, H.; Eidgahee, D.R.; Fakharian, P. Optimizing compressive strength prediction in eco-friendly recycled concrete via artificial intelligence models. *Multiscale Multidiscip. Model. Exp. Des.* **2024**, *8*, 24. [CrossRef]
86. Khodaparasti, M.; Alijamaat, A.; Pouraminian, M. Prediction of the concrete compressive strength using improved random forest algorithm. *J. Build. Pathol. Rehabil.* **2023**, *8*, 92. [CrossRef]
87. Wadhawan, S.; Bassi, A.; Singh, R.; Patel, M. Prediction of Compressive Strength for Fly Ash-Based Concrete: Critical Comparison of Machine Learning Algorithms. *J. Soft Comput. Civ. Eng.* **2023**, *7*, 68–110. [CrossRef]
88. Naderpour, H.; Rafiean, A.H.; Fakharian, P.; Naderpour, H.; Rafiean, A.H.; Fakharian, P.; Naderpour, H.; Rafiean, A.H.; Fakharian, P.; Naderpour, H.; et al. Compressive strength prediction of environmentally friendly concrete using artificial neural networks. *J. Build. Eng.* **2018**, *16*, 213–219. [CrossRef]

89. Hoang, N.D.; Tran, V.D. Deep Neural Network Regression with Advanced Training Algorithms for Estimating the Compressive Strength of Manufactured-Sand Concrete. *J. Soft Comput. Civ. Eng.* **2023**, *7*, 114–134. [CrossRef]
90. Saingam, P.; Hussain, Q.; Sua-Iam, G.; Nawaz, A.; Ejaz, A. Hemp Fiber-Reinforced Polymers Composite Jacketing Technique for Sustainable and Environment-Friendly Concrete. *Polymers* **2024**, *16*, 1774. [CrossRef] [PubMed]

Disclaimer/Publisher's Note: The statements, opinions and data contained in all publications are solely those of the individual author(s) and contributor(s) and not of MDPI and/or the editor(s). MDPI and/or the editor(s) disclaim responsibility for any injury to people or property resulting from any ideas, methods, instructions or products referred to in the content.